Inorganic Chemistry Communications 153 (2023) 110837

Contents lists available at ScienceDirect

Inorganic Chemistry Communications

journal homepage: www.elsevier.com/locate/inoche

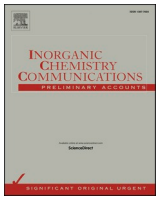

Short communication

Synthesis of low toxic silver-cobalt nanoparticles using *Annona muricata* leaf extract: Antimicrobial evaluation

Anuoluwa Abimbola Akinsiku [a,*], Ruth Opiotu Odaudu [a], Opeyemi Christianah De Campos [b], Alaba Oladipupo Adeyemi [b], Oluwaseun Ejilude [c]

[a] Department of Chemistry, Covenant University, Canaanland, Km 10 Idiroko Road, P.M.B. 1023 Ota, Ogun State, Nigeria
[b] Department of Biochemistry, Covenant University, Canaanland, Km 10 Idiroko Road, P.M.B. 1023 Ota, Ogun State, Nigeria
[c] Department of Parasitology, Sacred Hearts Hospital, Abeokuta, Ogun State, Nigeria

ARTICLE INFO

Keywords:
Antimicrobial agent
Annona muricata
Toxicity
Phytochemicals
Ag-Co nanoparticles

ABSTRACT

In a bid for green chemistry, a sustainable approach using *Annona muricata* aqueous extract was engaged as a reducing agent to synthesise bimetallic silver-cobalt nanoparticles (Ag-Co NPS). Hot extraction using distilled water was done on the locally sourced plant (leaf part). It was then screened for biomolecules present as geographical location affects phytochemical compositions. Phytoreduction reaction with nanoparticle formation rate was monitored with a UV–Vis spectrophotometer. Then, further characterisations were achieved by transmission electron microscopy (TEM), energy dispersive X-ray spectroscopy (EDX), Fourier-transform infrared (FTIR), and X-ray diffraction (XRD). The average particle size of 39.34 nm ± 9.21 nm was obtained. This study shows an interesting result, as the increase in Ag-Co NPs concentration did not significantly affect the flies' survival compared to the control. At $P < 0.05$, similar behaviour was observed in the locomotive assay of the model used. An antibacterial agent can also be developed, as revealed in the antimicrobial assay on *Staphylococcus aureus* (ATCC25923), *Streptococcus pneumoniae*, *Escherichia coli* (ATCC 25922), *Klebsiella* sp., and *Salmonella* sp. and a fungus strain: *Candida albicans*.

1. Introduction

Illness-causing organisms- bacteria, fungi, viruses, parasites, etc. have been identified as threats to humanity if their activities are not checked. This is one of the pivotal global issues ravaging the health sector. Unfortunately, these pathogens responsible for infectious diseases are drug-resisting. The current antibiotics are becoming less effective even with side effects, among others [1]. Finding an alternative to combat this menace is a necessity. A series of research is ongoing on developing new drugs and protocols to produce antimicrobial agents, leading to a paradigm shift in using nanomaterials for medical treatment.

Particles ranging between 1 and 100 nm in dimension (nanoparticles) possess unique properties, such as colour, variety in shape, increased surface area, and mechanical, optical, and magnetic properties. They are also chemically active and corrosion-resistant [2]. These engineered nanoparticles have been identified with the ability to have their surfaces manipulated or enhanced, which sets them apart from bulk materials. Nanoparticles are explored and studied in various fields due to their enhancing ability. Some are applied in medicine as drug delivery agents [3] and for strategic disease treatment. Nanomaterials in food science and technology provide improved alternative food packaging, foodborne pathogen detection (biosensing), and shelf-life extension [4,5]. However, the reported toxicity challenge posed by the nanomaterials may threaten humans and the environment plausibly based on the fabrication method, especially chemical and physical synthetic routes. Green synthesised nanoparticles are now explored by taking advantage of their high surface area to volume ratio [6], the simple procedure involved in the preparation, cost-effectiveness, and environmental friendliness due to sustainable materials used, and fewer toxicity concerns [7].

Plant-mediated nanoparticles are identified as suitable for drug delivery, photoelectronic, cosmetics, agriculture, and for therapeutic applications. It is worth knowing that some useful plant materials involved are geographically and seasonally available with different phytochemicals. The use of *Annona muricata,* known as soursop leaf, as a

* Corresponding author.
E-mail address: anu.akinsiku@covenantuniversity.edu.ng (A.A. Akinsiku).

https://doi.org/10.1016/j.inoche.2023.110837
Received 28 September 2022; Received in revised form 5 May 2023; Accepted 13 May 2023
Available online 16 May 2023

bioreduction agent is considered in this study. The plant is a tropical type that belongs to the Annonaceae family, located in tropical and subtropical geographical locations of the world. The leaf has been reported to be analgesic, anticonvulsant, anti-inflammatory, antioxidant, antihypertensive, wound healing, cytotoxic to tumour cells, etc. [8]. In a study by Badmus et al. [9], phytochemicals present in *A. muricata* were terpenoids, flavonoids, essential oils, saponins, alkaloids, and cyclopeptides, though they vary at different geographical locations. The presence of phytochemicals in plants is responsible for antimicrobial activities [10], and the reduction of metal ions. Not all plants support metal ion reduction based on their secondary metabolites' hydrophilic, amphiphilic, or hydrophobic nature [11].

Studies on plant-based green synthesis of mono, bimetallic, and iron oxide nanoparticles indicated their suitability for many applications. Deivanathan and Prakash [12] synthesised Ag NPs, 30 nm in size, that possessed antibacterial activity against *Streptococcus Aureus* (MTCC 273), *Escherichia coli* (MTCC 25,922), gram-negative bacterial and gram-positive bacteria, *Bacillus subtilis* (MTCC 2451) and *Staphylococcus Aures* (MTCC 25,923). Gold and silver nanoparticles for heavy metal detection were biosynthesised by Nayak et al. [13]. Elamin et al. [14] prepared NiO and Co-doped NiO nanoparticles with curry leaf that possessed antibacterial properties against Shigella *dysenteriae, Klebsiella pneumonia* (gram-negative) and *Bacillus subtilis* and *Staphylococcus aureus* (gram-positive) bacteria. Ag NPs using *Momordica charantia* stem extract were potent against *S. aureus, S. pyogenes, E. coli, P. aeruginosa, C. albicans,* and *T. rubrum* [15]. Bolade and others [16] synthesised iron oxide nanoparticles using *A. indica* that completely degraded soil contaminated with total petroleum hydrocarbons in the soil. Bimetallic Ag/Ni NPs were also reported as a potential candidate for antibacterial and antifungal agents using an abused plant, *Nicotiana tabacum* [17].

This research focused on synthesising silver-cobalt nanoparticles (Ag-Co NPs), characterisation, toxicity evaluation using the *Drosophila melanogaster* model, and antimicrobial assessment of pathogenic organisms. The previous study prepared its corresponding silver nanoparticles. *Annona muricata* leaf extract has not been reported to produce silver-cobalt nanoparticles (Ag-Co NPs); thus, the choice in this study. Characterisation of the biogenic nanoparticles was achieved with a UV–Visible spectrophotometer, Fourier-transform infrared (FTIR), and transmission electron microscope (TEM) to ascertain metal ion reduction, energy dispersive X-ray spectroscopy (EDX), and XRD for phase identification. The antimicrobial potential of the nanoparticles was also explored.

2. Experimental

2.1. Materials

Silver nitrate, cobalt nitrate hexahydrate, purchased from Sigma-Aldrich Corporation, U.K. *Annona muricata* leaf extract, distilled water, and filter paper (Whatman no.1).

2.2. Organisms

Two gram-positive bacteria (gram + ve): *Staphylococcus aureus* (ATCC25923) and *Streptococcus pneumoniae*; three (3) gram-negative bacteria (gram -ve), *Escherichia coli* (ATCC 25922), *Klebsiella sp*, and *Salmonella sp* and a fungus strain: *Candida albicans*. The control used–Bacteria- Ofloxacin (100 mg/mL) and *Candida* - Fluconazole (100 mg/mL).

2.3. Plant collection and preparation of extract

Annona muricata plant was collected from university premises and identified (Am/Bio/H844) by a botanist in the Department of Biological Sciences, Covenant University, Nigeria. The leaves were dried at ambient temperature for 14 days, washed, chopped, and blended. Hot extraction using water (as part of green chemistry) was done in a ratio of 1:10 w/v at 60–70 °C, and the broth was filtered with no. 1 Whatman filter paper. The filtrate was then collected and kept at 4°C for the synthesis of nanoparticles [18].

2.3.1. Phytochemical screening of Annona muricata leaf extract

The *Annona muricata* leaf extract was screened qualitatively to identify secondary metabolites using a standard technique [19].

2.4. Synthesis of silver-cobalt nanoparticles using the soursop leaf extract

An equal molar concentration (2 mM) of silver nitrate and cobalt nitrate hexahydrate was prepared separately in a 1-litre standard flask. The biosynthesis was carried out at 1:10 v/v plant extract to precursors, and the mixture was heated up with stirring to 70 °C for 60 min, resulting in a gradual colour change. Aliquot samples were taken every 10 min and checked for the appearance of surface plasmon resonance using a UV–Visible spectrophotometer. The colloid formed was centrifuged after the synthesis at 4000 rpm for 50 min, and then oven-dried for characterisation and further use [15].

2.5. Instrumental analyses

2.5.1. Sample characterisations

Optical analysis and bioreduction of Ag^{+} to Ag^{0} and Co^{2+} to Co^{0} were checked with Aquamate 8100 UV–Visible spectrophotometer. Absorption spectra of the aliquot samples were collected between 200 and 800 nm range using a Quartz cuvette operated at a resolution of 1 nm. The Blank used was distilled water. Functional groups responsible for the reduction process were analysed with Bruker FTIR Tensor 27 between 5000 and 500 cm^{-1} wavenumbers [20]. The sample's morphological properties and particle size were determined with the JEOL 1010 TEM instrument. Powdered X-ray diffraction studies were performed on a Bruker AXS D8 diffractometer using Cu-Ka radiation ($\lambda = 0.15418$ nm) at 40 kV, and 40 mA at room temperature. Scanning of the sample was done in the region of 20–90°, step size of 0.05 and a count of 10 s [21].

2.6. Toxicity assessment

Drosophila melanogaster model was used for the toxicity assessment with modification to the previous study [22]. The experiment began with culturing the *D. melanogaster* strain Harwich (wild type), obtained from a research laboratory in the Biochemistry Department, University of Ibadan, Nigeria (see details in supplementary 1). Pupation-rate tests were performed by reconstituting 5% bovine serum albumin at 0, 10, 20, 100, and 200 mg/mL. The number of emerging pupae was reported for five days. Then survival assessment was determined after modifying the methods described by Abolaji et al. [23]. The number of alive and dead flies was counted every day, and the information was then processed and represented as a percentage of dead flies. After the seven-day survival test, locomotive performance was measured. (See supplementary 1.1–1.17 for details).

2.7. Statistical analysis

Statistical analysis was done with Ordinary one-way ANOVA and Brown-Forsythe and Bartlett's test. The significant difference was considered when $p < 0.05$, and the data were expressed as mean ± SD. The figures were generated in GraphPad Prism 9.3.1 (GraphPad Software, Inc., San Diego, CA, USA).

2.8. Antimicrobial study of the synthesised Ag-Co NPs

2.8.1. Characterisation of bacterial isolates

Bacteria isolates (*Klebsiella* sp., *Salmonella* sp., and *Streptococcus pneumoniae*) and fungus isolates (*Candida albicans*) collected from

various hospitals in Abeokuta, western Nigeria, were identified morphologically and biochemically viz: gram staining, spore staining, capsule staining, motility, indole, citrate, urease, oxidase, catalase, coagulase, methyl-red and Voges–Proskauer (VP) and sugar fermentation test. The results were interpreted according to the Bergy Manual of Determinative Bacteriology [24]. Typed cultures: *Staphylococcus aureus* (ATCC 25923) and *Escherichia coli* (ATCC25922) were included in the assay. The following were carried out using standard procedures as described in previous work [25]: Gram staining, spore staining, capsule staining, catalase, coagulase, motility, indole test, citrate test, urease test, oxidase test, methyl-red (MR) test, Voger Proskauer (VP) test, and carbohydrate fermentation tests (see supplementary 2 for details of each test).

2.8.2. Antimicrobial activity

The well plate agar diffusion method was used to evaluate the nanoparticles' antimicrobial activity (see supplementary 2).

2.8.3. Minimum inhibitory concentration (MIC)

The MIC of the plant-based nanoparticles against the microbial isolates (including typed cultures) was determined using the microtubes dilution method described by National Committee for Clinical Laboratory Standards [26]. The resulting turbidity was observed after 24 h. Control for antimicrobial agents (Ofloxacin-Bacteria; Fluconazole-*Candida*) was included in the experiment (see supplementary 2).

2.8.4. Minimum bactericidal/fungicidal concentration (MBC/MFC) assay

Sub-culturing was made from each well that showed no growth from the MIC well onto chocolate agar (Bacteria) and malt extract agar (Candida) plates. Following overnight incubation at 37 °C in ambient air for 24 h, the plate was examined for the growth of bacteria and *Candida* colonies. Lack of growth indicated that the extract had bactericidal/fungicidal potential, while growth meant bacteriostatic/fungistatic activity [27].

3. Results and discussion

3.1. Phytochemical analysis

The secondary metabolites present in the aqueous extract of *A. muricata* leaf extract are presented in Table 1.

3.2. UV–Vis spectra analysis

The optical absorption analysis indicated $\pi \rightarrow \pi^*$ transition due to chromophores in the plant extract, which resulted in a gradual colour change in the reaction medium from white to brown, and this is visual evidence of nanoparticle formation (Fig. 1b). Also, during the optical measurement led to absorption peak with the appearance of surface plasmon band around 400–450 nm because of the free electrons on the Ag-Co NPs surface which oscillated collectively with incident light. This confirmed formation of nanoparticles with a characteristic silver absorption wavelength. This observation contrasted with the corresponding Ag NPs (428 nm) (Fig. 1c) and a previous study where Ag NPs were formed at 420 nm using *A. muricata* as a reducing agent [9]. The red shift observed in this work may be plausibly due to aggregation between nanoparticles resulting in large particle sizes, also tunable SPR due to the synergistic effect of the bimetallic nanoparticles compared to the monometallic metal nanoparticles [28]. Fig. 1 (c) shows the comparative absorption spectra of Ag, Co, and Ag-Co NPs, showing the synergetic effect of cobalt in the red-shifted Ag-Co NPs with increased absorption intensity compared to its corresponding Ag NPs with 428 nm wavelength of absorption. However, there was no surface plasmon resonance in the absorption spectrum of the extract; it only aided $\pi \rightarrow \pi^*$ transition because of its chromophoric nature [4]. The EDX analysis indicated the formation of bimetallic Ag-Co NPs with the predominating atomic composition of silver (29.54%) and cobalt (20.87%). The carbon present originated from the plant extract, as shown in Fig. 2.

Significant absorption occurred in 10 min when the first SPR appeared, confirming nanoparticle formation. Higher absorption intensity than its corresponding Ag NPs was observed (Fig. 1c), which increased with time, maximum at 50 min (2.70 a.u.). The almost overlapping spectra suggested that the reaction tended towards completion. There was no SPR in the cobalt nanoparticle (Fig. 1a). This observation is different from conventional protocols that elongate the reaction time for nanoparticle formation, which has been a challenge. In addition, the reaction also indicated that the phytochemicals in *A. muricata* aqueous extract were adequate to reduce Ag^{+} to Ag^{0} and Co^{2+} to Co^{0}; however, there is still a need to identify the compound in the extract responsible for this reduction. The shapes of the absorption spectra in Fig. 1a suggest the formation of spherical nanoparticles.

Table 1
Preliminary phytochemical screening of aqueous *A. muricata* leaf extract.

Phytochemicals	Presence
Carbohydrate	+
Alkaloids	++
Terpenoids	–
Flavonoids	+
Glycosides	–
Quinone	+
Phenols	++
Cardiac glycoside	+
Coumarins	–
Ninhydrin	+
Tannins	–

Present (+), absent (-).

3.3. Fourier-transform infrared (FTIR) analyses of A. Muricata plant and allied Ag-Co NPs

The functional groups present in the plant-based Ag-Co NPs and the *Annona muricata* leaf extract are shown in Fig. 3. The analysis showed the moieties (O–H, N–H, C-N, C-O, and C–H) available in the phytochemicals that capped the nanoparticles after synthesis, thus, providing stability. Table 2 shows the designation of functional groups to bands at different wavenumbers, functional groups in the plant-based Ag-Co NPs and the *A. muricata* leaf extract. A significant reduction in the band intensity of *A. muricata* aqueous extract compared to that of the Ag-Co NPs at different wavenumbers is observed. Of course, this is due to silver and cobalt acting on the coordination via the nitrogen present in the alkaloids. The identified broad peak in the Ag-Co NPs at 3322 cm^{-1} is assigned to N–H stretching in alkaloids or O–H stretching of flavonoids or phenols phytochemicals which acted as the reducing and capping agent during the reaction. The peak 1585 cm^{-1} to N–H bending of amine, 1400 cm^{-1} to O–H stretching of alcohol, 1277 cm^{-1} weak stretch to C-O stretch, and 1046 cm^{-1} to C-O stretching present in the cardiac glycosides. However, the observed O–H stretching present in the FTIR *A. muricata* ascribed to flavonoids or phenols present in the *A. muricata* leaf extract is intensified in Ag-Co NPs as indicated in the spectrum (Fig. 2b), like the FTIR analysis of the corresponding Ag NPs formation in the previous study [9]. The intensity of the absorption band, 1585 cm^{-1} assigned to N–H bending of amine, in the alkaloids is still present in the Ag-Co NPs with strong intensity, in contrast to that of the extract with weak intensity (1649 cm^{-1}N–H bending, and 1163 cm^{-1}C-N weak stretching of amine) in the extract. Hence, this analysis suggests that O–H (in glycosides, flavonoids, phenol, and carbohydrates), N–H and C-N (in alkaloids) might have reduced Ag^{+} to Ag^{0} and Co^{2+} to Co^{0} and adsorbing of the surface of the nanoparticles thereby providing stability. An experiment is underway to identify the compounds in the *A. muricata* responsible for reducing metal ions in forming Ag-Co NPs. The proposed

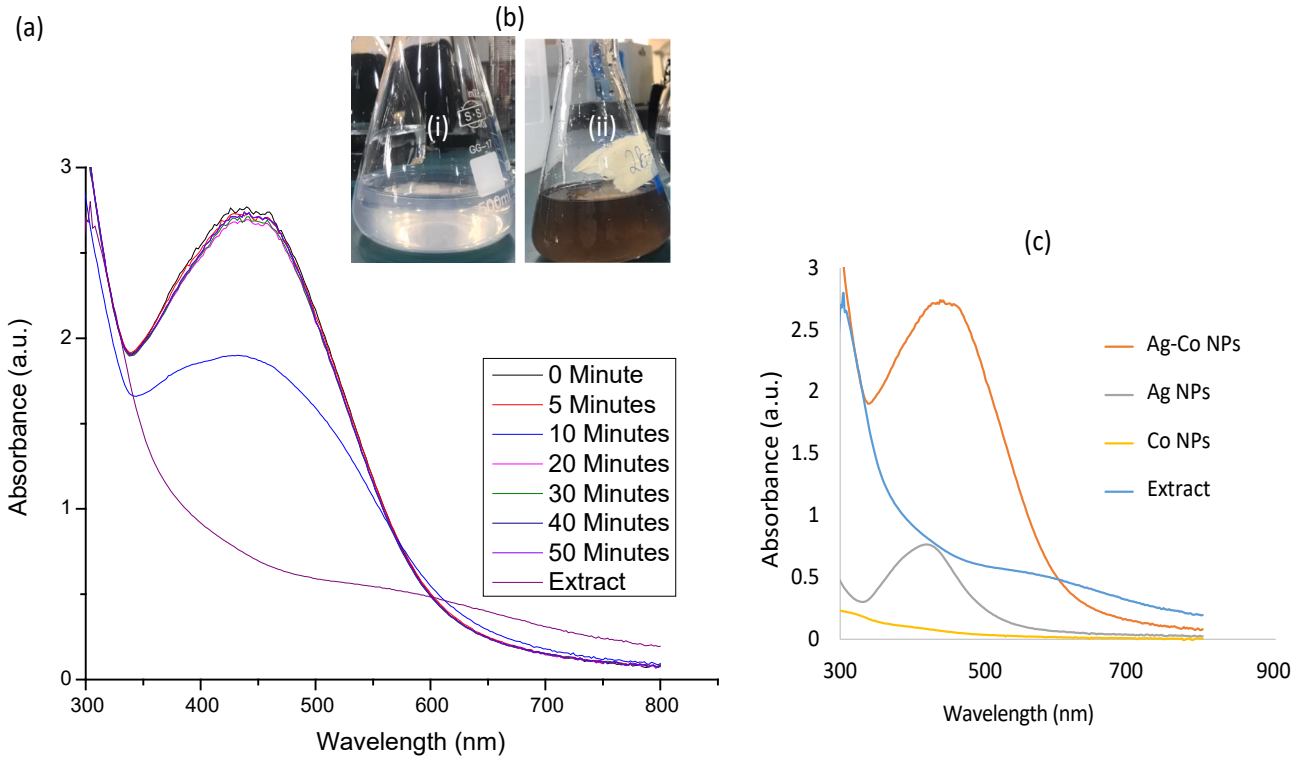

Fig. 1. (a) Combined UV–Visible spectra of Ag-Co NPs at 70 °C (b) (i) Colour formation before and (ii) final dispersion after reduction (c) A comparative absorption spectrum of Ag, Co, Ag-Co NPs.

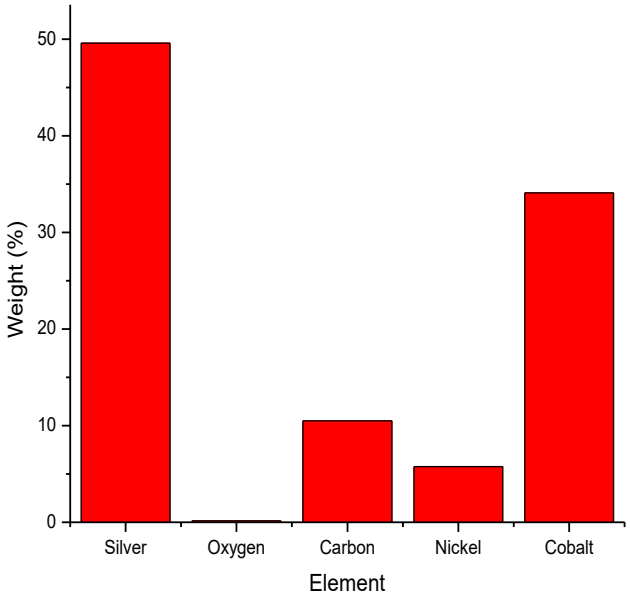

Fig. 2. EDX of *A. muricata*-based Ag-Co NPs.

reduction mechanism is presented in Scheme 1.

3.4. TEM analysis

TEM representation at different resolutions and the corresponding distribution of the Ag-Co NPs are shown in Fig. 4. The particle size ranges between 9.50 and 63.58 nm with an average size of 39.34 nm ± 9.21 nm (Using Image J software). The particles were pseudo-spherically shaped, a common morphology of plant-oriented nanoparticles. The Ag-Co NPs were smaller when compared with the corresponding Ag NPs using *A. muricata* as a reducing agent [9,29]. This observation could be attributed to the effect of cobalt. However, no literature was found to compare the hybrid using soursop leaf as a green reducing agent. The TEM micrographs reveal aggregated alloy nanoclusters plausibly due to the nature of the reducing agent used, which varies from plant to plant [30].

3.4.1. Powder X-ray analysis

Fig. 5a is the representative XRD pattern of the green synthesised Ag-Co bimetallic nanoparticles, as revealed in the result. The diffraction indicates reflections at 2 θ values of 32.50° (220, Co), 38.45° (111, Ag), and 64.82° (220, Ag). The identified reflection planes of (111) and (220) correspond to Ag with a face-centred cubic structure, while plane (220) corresponds to Co [31]. The remaining unidentified peaks in the diffractogram show the presence of an impure phase or mixture. This may be due to the biogenic nature of the reducing agent, *Annona muricata*, where the macro elements might be nanostructured. This observation is common to green-synthesised nanoparticles, especially when plant extract serves as capping or reducing agent A similar trend is found in the study by Patra & Baek (2016) [32]. The average crystallite size calculated from peaks is 38.46 nm, using, $D = \frac{0.94\lambda}{\beta Cos\theta}$. Where D = particle size, $\lambda = 0.154nm, \beta = FWMH = 0.4425$, obtained from Origin software, and converted to radian, 2θ = diffraction angle. The d-interspacing obtained = 0.2338 nm, using $d = \frac{\lambda}{2\sin\theta}$.

Similar crystallographic matches were obtained for the green synthesised Ag NPs and Ag-Co NPs, matched with COD #96-901-1667 (Fig. 5b&5c). The pattern matched the chlorargyrite phase with cell parameter, a = 5.54630 Å, space group $Fm^{-3}m$ (225) [33]. The diffraction pattern of the *A. muricata*-based Ag NPS (Fig. 5b) shows a cubic phase with five characteristics reflection peaks at 2 θ values of 29.99°, 32.41°, 46.39°, 55.00°, and 57.60°, which correspond to the lattice planes (111), (200), (220), (311), and (222), respectively [33].

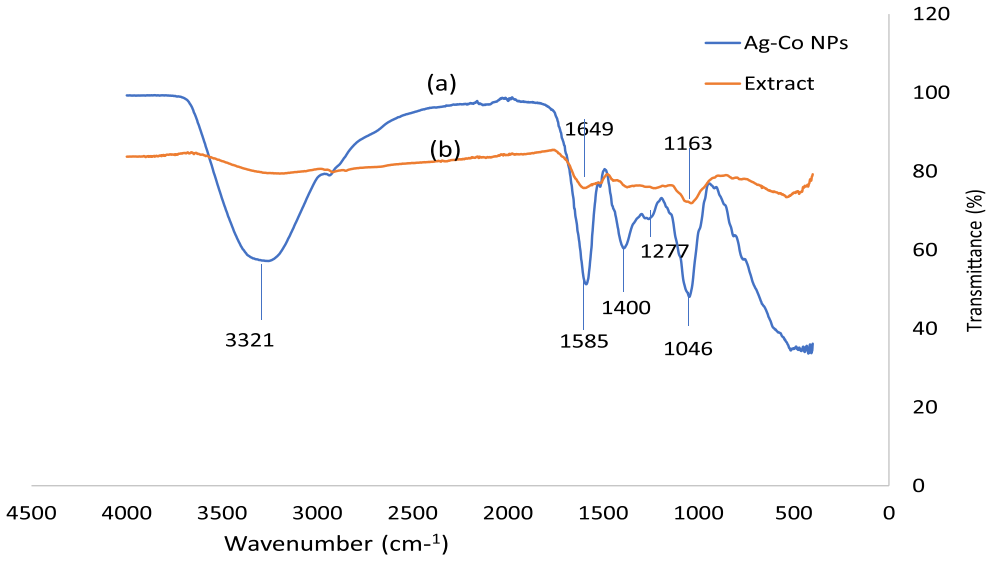

Fig. 3. FTIR spectral of (a) Ag-Co NPs and (b) *Annona muricata* leaf extract.

Table 2
FTIR absorption bands for *Annona muricata* aqueous leaf extract and corresponding Ag-Co NPs.

Ag-Co NPs			*Annona muricata* extract		
Absorption Intensity	Absorption bands (cm^{-1})	Functional group	Absorption Intensity	Absorption bands (cm^{-1})	Functional group
Broad	3322	O–H			
Sharp	1585	N–H	Very broad	1649	N–H
Medium	1400	O–H			
Weak	1277	C-N	Weak	1163	CH_3
Sharp	1046	C-O			

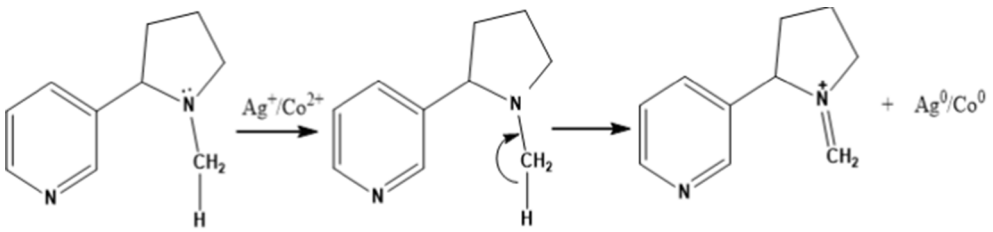

Scheme 1. Proposed phyto reduction of Ag^{+} /Co^{2+} to Ag^{0}/Co^{0} by alkaloids.

3.5. Toxicity evaluation of A. muricata-based Ag-Co NPs using Drosophila melanogaster model

The toxicity of nanoparticles was previously reported to affect metabolic activities, cell viability, and proliferation rate; it even distorts therapeutic effectiveness [34]. The as-synthesised Ag-Co NPs in this study were tested on the two developmental stages of Harwich wild-type *Drosophila melanogaster*. Possible effects of the Ag-Co NPs were checked on the growth of *D. melanogaster* by comparing the mean pupation after 5 days of treating 2nd instar larvae with different concentrations of green synthesised Ag-Co NPs with the control as presented in Fig. 6a. Findings from this study showed that 2nd instar larvae that were treated with 10, 20, 100, and 200 mg/L of green synthesised Ag-Co NPs within 5 days had a decrease in the numbers of pupated larvae when compared to the control. However, this decrease was not statistically significant ($P > 0.05$) compared to the control. A previous study showed that the larva stage of the flies had the most accumulation of nanoparticles, which may prevent them from pupating. Nevertheless, the particles did not significantly affect their pupation stage in this investigation. It revealed a healthy transition from larvae to the pupa stage, where a large accumulation of nanoparticles was mostly found in the larva, which prolonged their growth [35].

In addition, the survival assay was conducted to study how flies survived on a diet spiked with nanoparticles (Fig. 7). Remarkably, the assay result showed no observable difference in the survival rate at the different treatment doses compared to the control. The increase in concentration did not adversely affect the flies' survival rate compared to the control containing standard feed. At $P < 0.05$, a similar result was observed in the locomotive assay.

Negative geotaxis assay refers to measures of the locomotive performance of adult fruit flies. It describes adult fruit flies' upward flight when tapped to the bottom of a test tube. This work's negative geotaxis assay result showed a significant increase in the locomotive performance of adult flies treated with 20 mg/L of Ag-Co NPs compared to the control (Fig. 8). A sharp decrease, which was not statistically significant at higher concentrations of 100 and 200 mg/L, was also observed compared to the control. Hence, the findings from this study suggest that green synthesised Ag-Co NPs at 20 mg/L improved the locomotive behaviour of adult fruit flies.

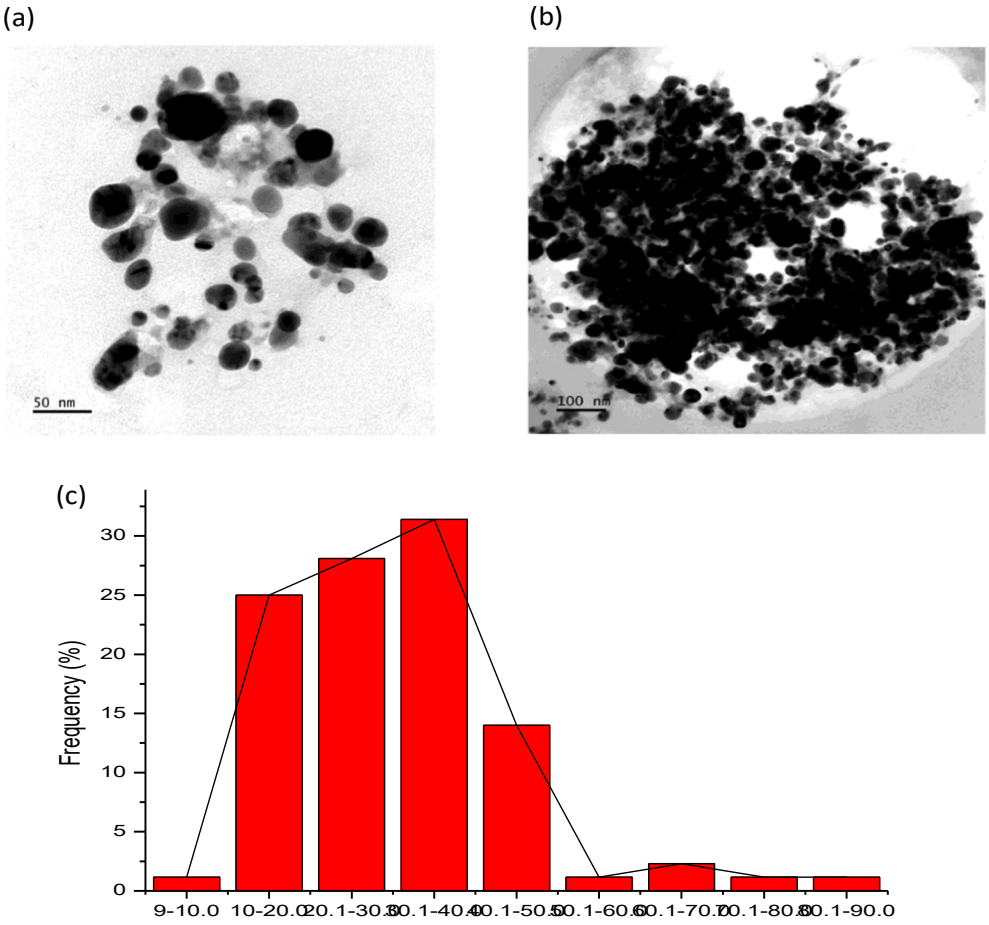

Fig. 4. TEM micrographs at different resolutions (a-b), Corresponding particle size distribution determined from TEM(c).

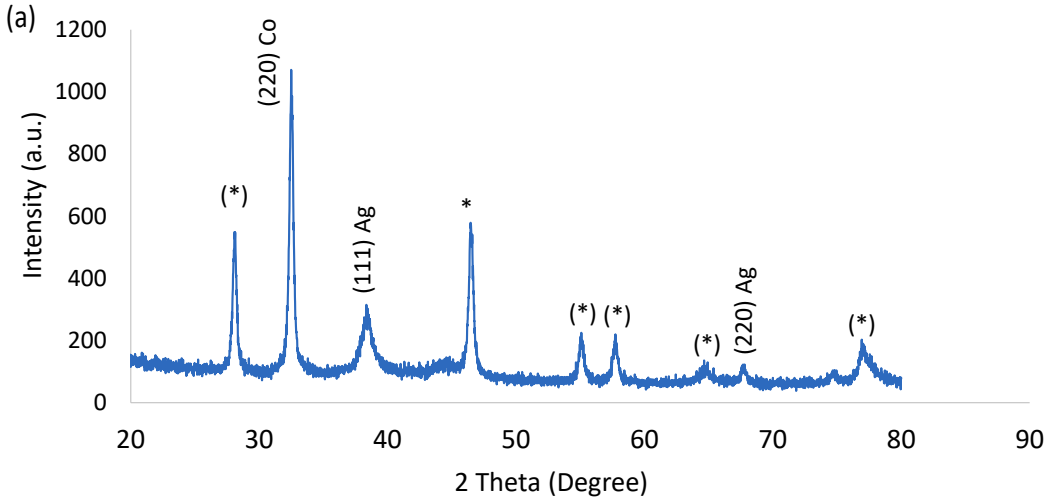

Fig. 5a. Representative pXRD pattern of the *A. muricata*-based Ag-Co NPs.

3.6. Antimicrobial activity

Results of sensitivity testing of organisms using agar diffusion test with standard deviation in zones of inhibition are revealed in Table 3 and Fig. 9. The result showed that both *A. muricata* extract and the bio-inspired Ag-Co NPs inhibited the growth of the test organisms. As in the previous study, *A. muricata*-based Ag-Co NPs possessed antibacterial and antifungal activities [36]. The antimicrobial activity study of *A. muricata*-based Ag-Co NPs was carried out on two gram-positive bacteria (gram + ve): *Staphylococcus aureus* (ATCC25923), *Streptococcus pneumoniae*, three-gram negative bacteria (gram -ve), *Escherichia coli* (ATCC 25922), *Klebsiella sp*, and *Salmonella sp* and a fungus strain: *Candida albicans*. The control used– Bacteria- Ofloxacin (100 mg/mL) and *Candida*- Fluconazole (100 mg/mL).

A. muricata leaf extract was also tested for antibacterial activity and compared to Ag-Co NPs. The *A. muricata* leaf extract and its

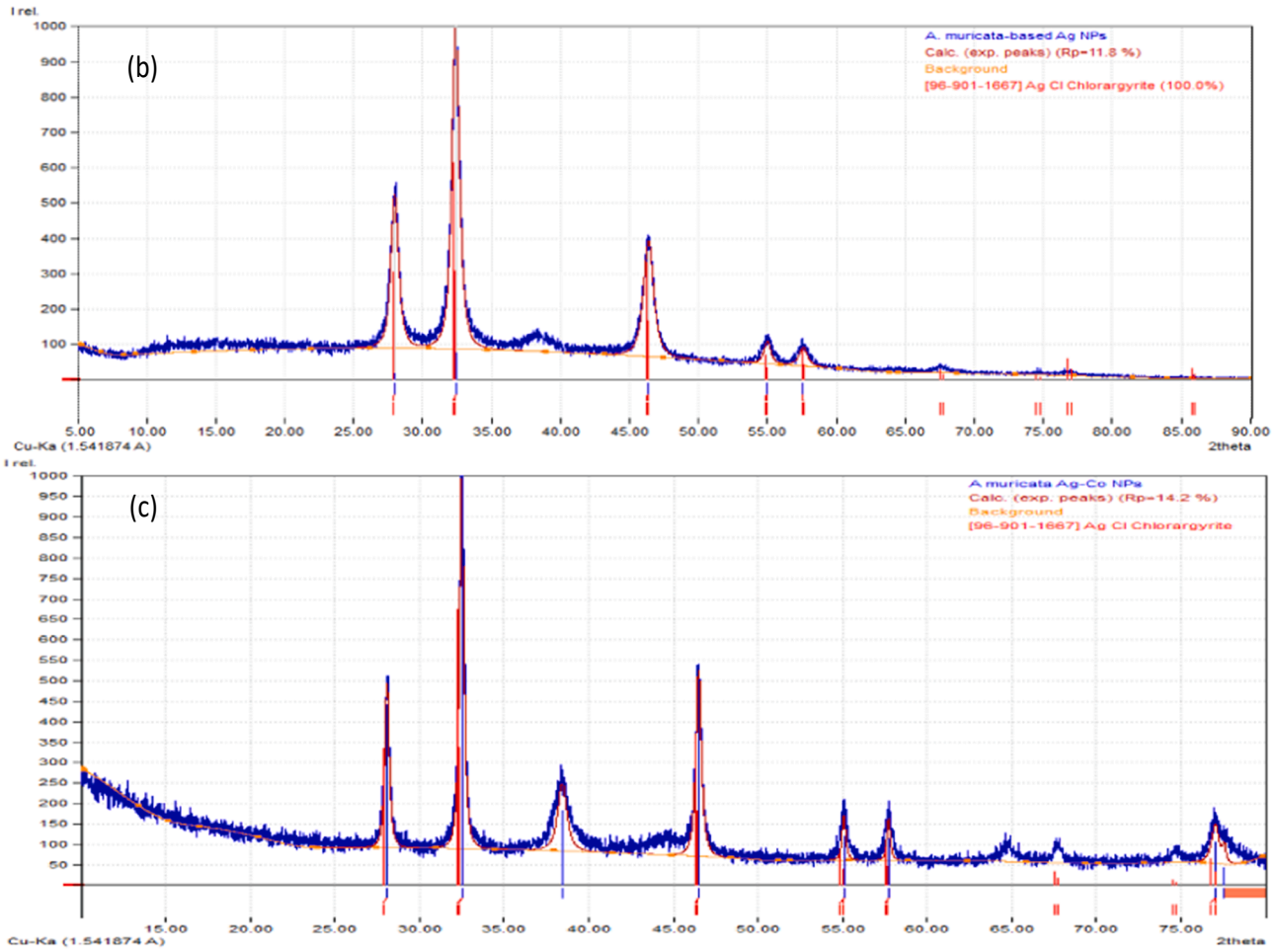

Fig. 5b. XRD pattern of the chlorargyrite phase *A. muricata*-based Ag NPs (c) *A. muricata*-based Ag-Co NPs.

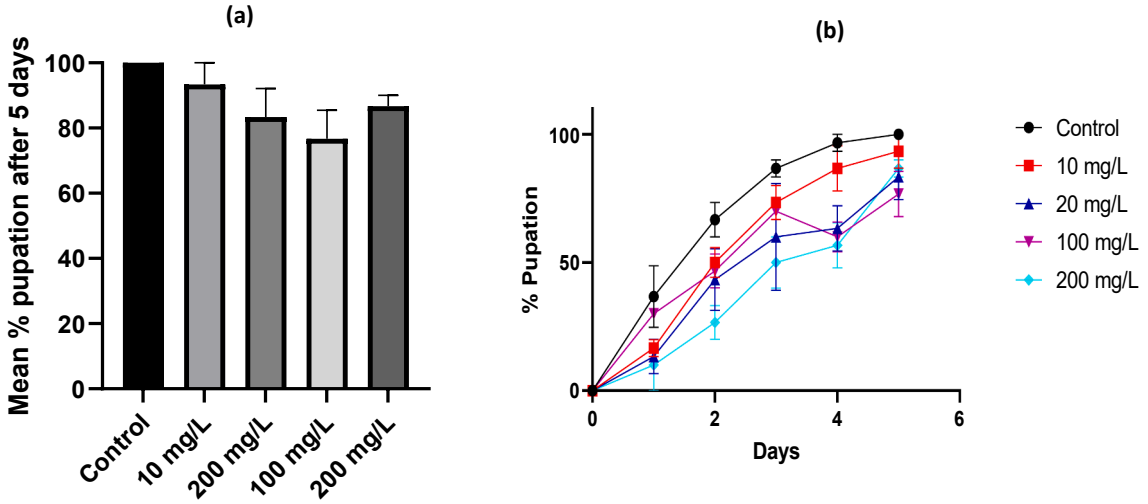

Fig. 6. Comparison of (a) mean % pupation after 5 days of treating 2nd instar larvae with different concentrations of green synthesised Ag-Co NPs and the control n = 10, (b) percentage pupation in control and the different concentration of green synthesised Ag-Co NPs within 5 days of treatment, n = 10. (For interpretation of the references to colour in this figure legend, the reader is referred to the web version of this article.)

corresponding bimetallic nanoparticles possess antimicrobial properties. The potency was so strong when compared with the control (Ofloxacin). Moreso, the highest zone of inhibition and activity was displayed by Ag-Co NPs (average, 23.5 mm) and the extract (average, 22.5 mm) against *Escherichia coli*, as gram-negative bacteria were found to be more susceptible to nanoparticles than the gram-positive ones due to their cell wall composition (thin lipopolysaccharides, phospholipids, and lipoprotein) [17], compared to the control with the average inhibition zone of 26.5 mm. The next inhibition potency was observed in *Staphylococcus aureus* (Ag-Co NPs 20.5 mm, extract 17.5 mm) compared

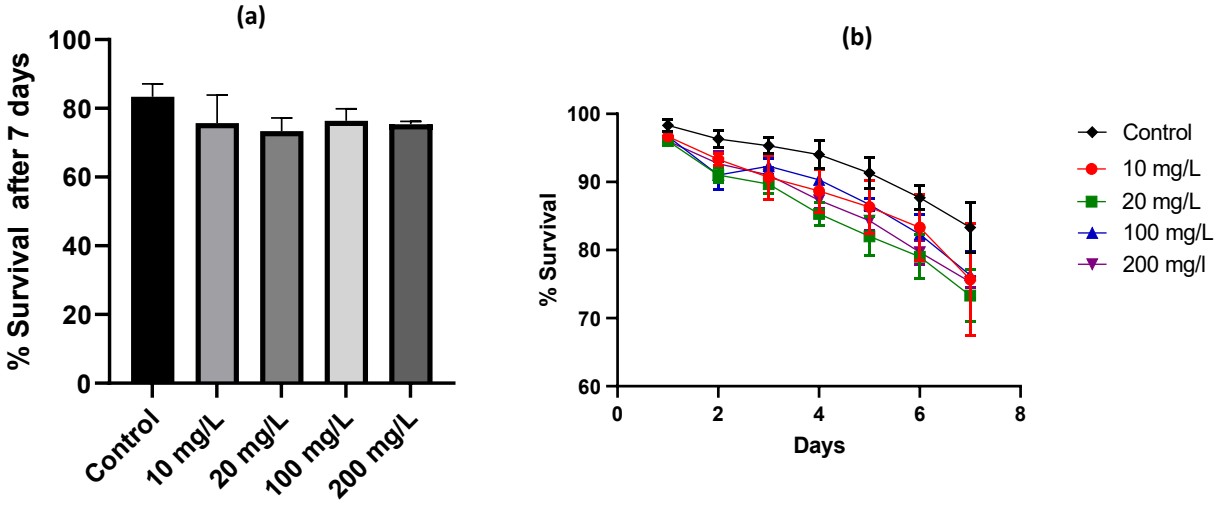

Fig. 7. Comparison of (a) mean survival of flies exposed to different concentrations of Ag-Co NPs and control after 7 days, n = 10, (b) percentage survival of flies within 7 days of treatment with control and different concentrations of Ag-Co NPs, n = 10. P > 0.05.

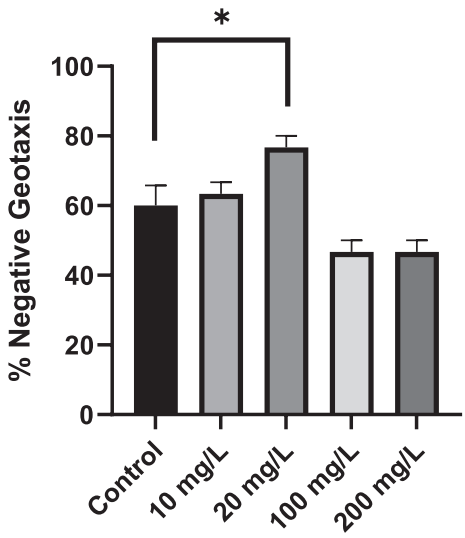

Fig. 8. Comparison of percentage locomotion performance after 7-day survival test. Bars with * are significantly different at P < 0.05.

to ofloxacin, 26.5 mm, *Klebsiella* sp. (Ag-Co NPs 19 mm, extract 13.5 mm), compared to 25.5 mm by ofloxacin, *Streptococcus pneumoniae* (Ag-Co NPs 17 mm, extract 17.5 mm), control 26.5 mm. Followed by *Salmonella* sp. (Ag-Co NPs 15.5 mm, extract 15 mm), control 27.5 mm. And the last activity on *Candida albicans* (Ag-Co NPs 12.5 mm, extract 10.5 mm), control 25.5 mm inhibition (Fig. 8).

The results of the MIC (the lowest concentration of antimicrobial agent that will inhibit the visible growth of an organism) of Ag-Co NPs, *A. muricata* leaf extract, and the control (ofloxacin) are presented in Table 3 and Fig. 10. According to Gurunathan et al. [37], NPs with smaller sizes were documented to improve antimicrobial activity due to their large surface area to volume ratio that enhances strong interaction area and intracellular penetration. Interestingly, both the nanoparticles and the leaf extract had activity. The highest MIC with the same average concentration of 6.25 mg/mL was observed in Ag-Co NPs and *A. muricata* leaf extract against *Escherichia coli* and *Staphylococcus aureus* (most susceptible) compared to ofloxacin (3.13 mg/mL). For the antimicrobial mechanism, it is possible that Ag-Co NPs infiltrated teichoic and the pores on the cell wall of *S. aureus* (Gram + ve bacterium) because the NPs (Ag^o/Co^o) could not hold to the negatively charged peptidoglycan layer of the bacterium cell wall [38], leading to generation of reactive active species (ROS) that interrupted the production of adenosine triphosphate resulting in the microorganism cell death [39].

Amazingly, the succeeding activity was observed in the aqueous leaf extract of *A. muricata* at 6.25 mg/mL concentration, the same as the control, against *Staphylococcus aureus*. Then by the activity of Ag-Co NPs (12.5 mg/mL) and leaf extract 6.25, 12.5 mg/mL) against *Klebsiella* sp. The Ag-Co NPs and the extract at the same concentration (12.5, 12.5 mg/mL) revealed the next activity against *Salmonella* sp. and *Streptococcus pneumoniae.* The least MIC against *Candida albicans* was observed in Ag-Co NPs (50.0 mg/mL) and the extract at 50.0 mg/mL concentrations compared to the control at 6.25 and 3.13 mg/mL concentrations.

Results of the test to determine the lowest concentrations of antibiotic agents to kill at least 99.9% of microorganisms (MBC) are shown in Table 3 and Fig. 11. The highest activity was still observed against *Escherichia coli* and *Staphylococcus aureus* by *A. muricata* leaf extract with a similar concentration as the control, 6.25 mg/mL. Next was the

Table 3
Sensitivity testing with standard deviation in zones of inhibition (Agar Diffusion Test).

	Gram-negative strains *Escherichia coli* (ATCC 25922)		*Klebsiella sp*		*Salmonella sp*		Gram-positive strains *Staphylococcus aureus* (ATCC25923)		*Streptococcus pneumoniae*		Fungus strain *Candida albicans*	
	Zone diameter (mm)											
	T1,	T2	T1,	T2	T1,	T2	T1,	T2	T1,	T2	T1,	T2
Ag-Co NPs	25.0,	22.0	20.0,	18.0	15.0,	16.0	21.0,	20.0	18.0,	16.0	11.0,	14.0
Annona muricata leaf extract	22.0,	23.0	15.0,	12.0	16.0,	14.0	13.0,	12.0	17.0,	18.0	10.0,	11.0
Control	26.0,	27.0	25.0,	26.0	28.0,	27.0	25.0,	27.0	26.0,	27.0	25.0,	26.0

Control – Ofloxacin (100 mg/ml), T1 = Test 1, T2 = Test 2.

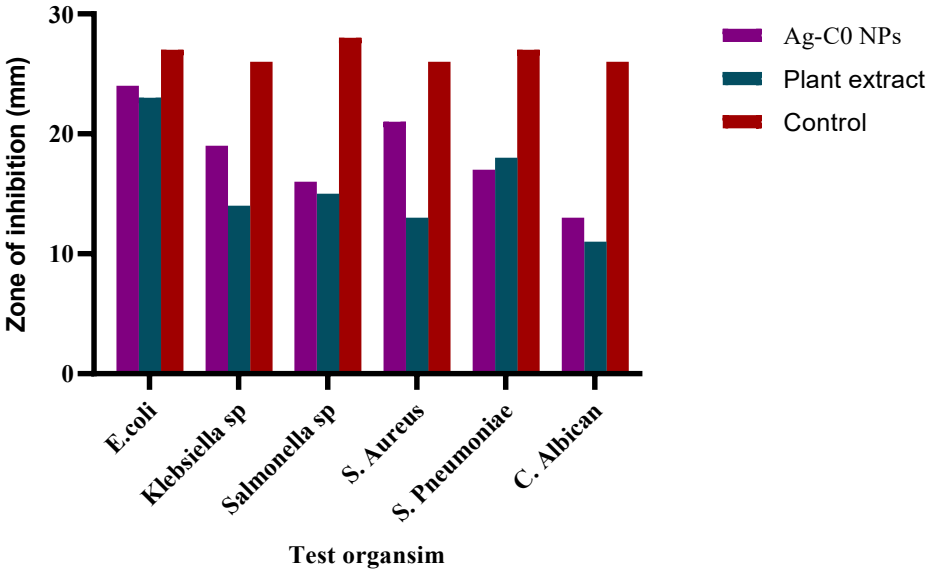

Fig. 9. Comparison of the zones of inhibition among *A. muricata* – mediated Ag-Co NPs, *A. muricata* leaf extract, and the control (Ofloxacin).

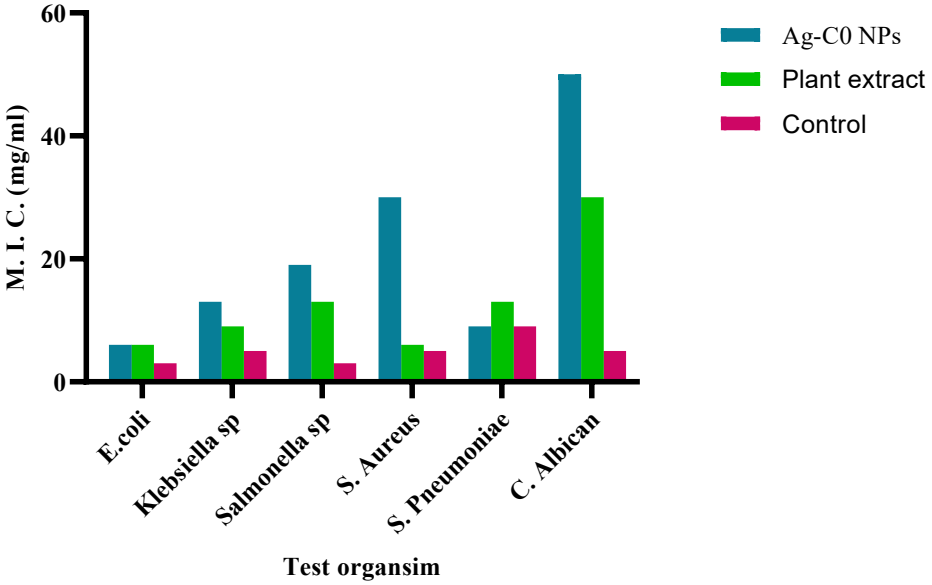

Fig. 10. MIC comparison of the test organism among Ag-Co NPs, A. *muricata* leaf extract and the control (Ofloxacin).

activity against *Streptococcus pneumoniae* by Ag-Co NPs (12.5 mg/mL) and the extract (12.5, 25.0 mg/mL). Then, the activity against *Klebsiella* sp. by the leaf extract (12.5 mg/mL) and Ag-Co NPs (25.0, 12.50 mg/mL). The extract exhibited subsequent activity against *Salmonella sp*. (12.50. 25.0 mg/mL) and the Ag-Co NPs (25.0 mg/mL). Least activities by the Ag-Co NPs and the extract compared to the control were observed in the minimum fungicidal concentration (MFC) test carried on against *Candida albicans* by *A. muricata* leaf extract (50.0 mg/mL) and Ag-Co NPs (100.0, 50.0 mg/mL) (Fig. 12). The ANOVA statistical analysis revealed $P < 0.05$ significant level. Thus, the findings revealed that gram + ve and gram -ve bacteria in this study were more susceptible to the extract and Ag-Co NPs than the fungus due to the complex resistivity of fungal strains [39].

4. Conclusion

This study explored the bioreduction potential of soursop leaf extract for the first time in synthesising Ag-Co NPs. Nanoparticle formation was initially confirmed with a UV–Vis spectrophotometer, supported by TEM, FTIR, EDX, and XRD. Small-size nanoparticles (average 39.34 nm ± 9.21 nm) were obtained compared to corresponding Ag NPs in the previous study. The antimicrobial analysis showed that the extract and the as-prepared Ag-Co NPs are good antibacterial agents against *E. coli.* and *S. aureus* compared to the control, with an average activity against other bacteria. The least activities by the Ag-Co NPs and the extract compared to the control were observed in the minimum fungicidal concentration (MFC) test carried on against *Candida albicans.* In contrast to toxicity threats posed by nanoparticles, especially those fabricated using conventional techniques, the green synthesised Ag-Co NPs using *A. muricata* aqueous leaf extract exhibited low significant toxic effect ($P < 0.05$) on the three developmental stages of *D. melanogaster* tested within the scope of this study. Further work is required to check the respiratory effect on living systems and any oxidative stress on *D. melanogaster* for pharmaceutical use and identify the compounds in the bioreducing agent.

Authors contributions

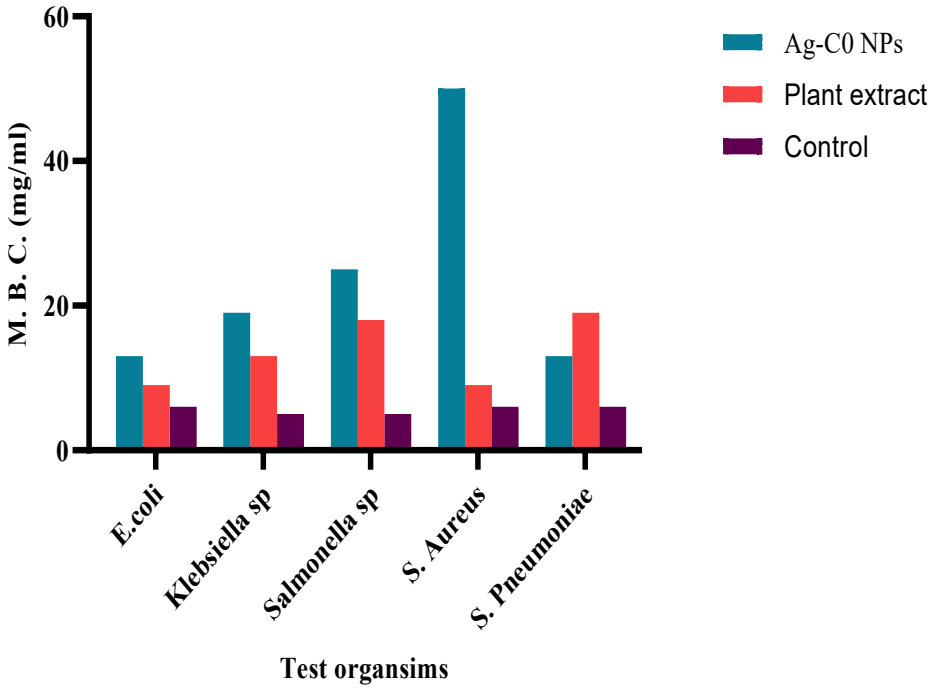

Fig. 11. MBC comparison of the test organism among Ag-Co NPs, *A. muricata* leaf extract and the control (Ofloxacin).

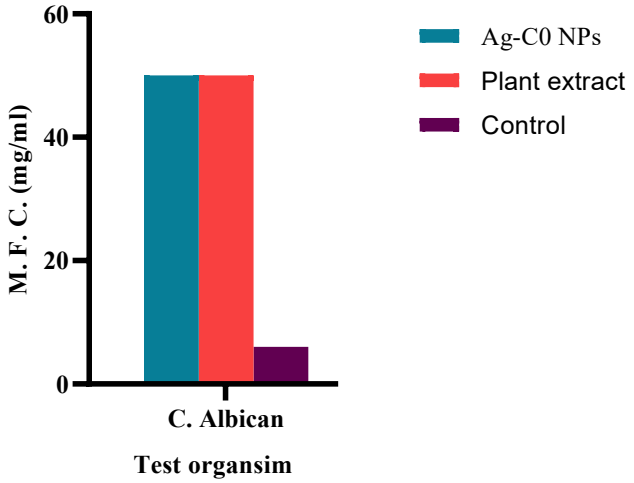

Fig. 12. MFC comparison of the test organism among Ag-Co NPs, *A. muricata* leaf extract and the control (Ofloxacin).

All authors contributed to the study. A.A. Akinsiku designed the research. R.O. Odaudu experimented. O.C. De Campos did a toxicity assay. A.O. Adeyemi handled part of the data analysis. O. Ejilude carried out the antimicrobial assay. A.A. Akinsiku revised the manuscript.

Funding

The authors did not receive support from any organisation for the submitted work.

Compliance with Ethical Standards

We declare that any fund granted to this research cannot affect the outcome of this manuscript submission.

Declaration of Competing Interest

The authors declare that they have no known competing financial interests or personal relationships that could have appeared to influence the work reported in this paper.

Data availability

The datasets to this manuscript are uploaded to Mendeley data.

Appendix A. Supplementary material

Supplementary data to this article can be found online at https://doi.org/10.1016/j.inoche.2023.110837.

References

[1] F.A. Zadeh, D.O. Bokov, O.D. Salahdin, Cytotoxicity evaluation of environmentally friendly synthesis copper/zinc bimetallic nanoparticles on MCF-7 cancer cells, Rend. Fis. Acc. Lincei. 33 (2022) 441–447, https://doi.org/10.1007/s12210-022-01064-x.

[2] N.N. Bonnia, M.S. Kamaruddin, M.H. Nawawi, S. Ratim, H.N. Azlina, E.S. Ali, Green biosynthesis of silver nanoparticles using 'polygonum hydropiper' and study its catalytic degradation of methylene blue, Procedia Chem. 19 (2016) 594–602, https://doi.org/10.1016/j.proche.2016.03.058.

[3] C. Lopez-Chaves, J. Soto-Alvaredo, M. Montes-Bayon, J. Bettmer, J. Llopis, C. Sanchez-Gonzalez, Gold nanoparticles: distribution, bioaccumulation and toxicity. In vitro *and* in vivo *studies.* Nanomedicine. 14 (2018) 1–12. https://doi.org/10.1016/j.nano.2017.08.011 10.1016/j.nano.2017.08.011.

[4] K. Saravanakumar, X. Hu, R. Chelliah, D.H. Oh, K. Kathiresan, M.H. Wang, Biogenic silver nanoparticles-polyvinylpyrrolidone based glycosomes coating to expand the shelf life of fresh-cut bell pepper (*Capsicum annuum L. var. grossum (L.)* Sendt). Postharvest Biol. Technol. 160 (8) (2020) 111-039. https://doi.org/10.1016/j.postharvbio.2019.111039.

[5] V. Suvarna, A. Nair, R. Mallya, T. Khan, A. Omri, A, Antimicrobial nanomaterials forfood packaging, Antibiotics. 11 (2022) 729, https://doi.org/10.3390/antibiotics11060729.

[6] S.O. Alayande, A.A. Akinsiku, A.A., Akinsipo, O.B., Ogunjinmi, E.O. Dare, Green synthesized nanomaterials and their therapeutic applications. Compr. Anal. Chem. Elsevier (Book Chapter). (2021). http://ir.tech-u.edu.ng/id/eprint/1101.

[7] A. Velidandi, S. Dahariya, N.P.P. Pabbathi, D. Kalivarathan, R.R. Baadhe, A review on synthesis, applications, toxicity, risk assessment and limitations of plant extracts synthesized silver nanoparticles, NanoWorld J. 6 (3) (2020) 35–60, https://doi.org/10.17756/nwj.2020-079.

[8] A.K. Oyebamiji, G.F. Tolufashe, O.M. Oyawoye, T.A. Oyedepo, B, Semire, Biological The activity of selected compounds from A*nnona muricata* seed as anti-breast cancer agents: theoretical study, J Chem. vol. 2020, Article ID 6735232, 10 pages, 2020. https://doi.org/10.1155/2020/6735232.

[9] J.A. Badmus, S.A. Oyemomi, O.T. Adedosu, T.A. Yekeen, M.A. Azeez, E. A. Adebayo, A. Lateef, U.M. Badeggi, S. Botha, A.A. Hussein, J.L. Marnewick, Photo-assisted bio-fabrication of silver nanoparticles using Annona muricata leaf

extract: exploring the antioxidant, anti-diabetic, antimicrobial, and cytotoxic activities, Heliyon 6 (2020) https://doi:10.1016/j.heliyon.2020.e05413.
[10] I.O. Olanrewaju, R.C. Mordi, J.O. Echeme, Antibacterial, antifungal and anti-tubercular activities of chloroform fraction of the leaf extract of *Irvingia Gabonensis* (African bush mango), Anti-Infect. Agents. 18 (2) (2020) 109–114, https://doi.org/10.2174/2211352517666181122125411.
[11] K. Mehrdad, Q. Hajar, M.S. Alijani, S.V. Rajender, Core@Shell Nanoparticles: greener synthesis using natural plant products, Appl. Sci. 8 (2018) 411, https://doi:10.3390/app8030411.
[12] S.K. Deivanathan, J.T. Joseph, Green synthesis of silver nanoparticles using aqueous leaf extract of Guettarda speciosa and its antimicrobial and anti-oxidative properties, Prakash Chem. Data Collect. 38 (2022) https://doi.org/10.1016/j.cdc.2022.100831.
[13] S. Nayak, L.C. Goveas, P.S. Kumar, R. Selvaraj, R. Vinayagam, Plant-mediated gold and silver nanoparticles as detectors of heavy metal contamination, Food Chem. Toxicol. 167 (2022), 113271, https://doi.org/10.1016/j.fct.2022.113271G.
[14] N.Y. Elamin, T. Indumathi, E.R., *Murayya koenigii* mediated synthesis of cobalt doped NiO nanoparticles: Evaluation of structural, optical properties and anti-bacterial activity Physica E Low Dimens, Syst. Nanostruct. 142 (2022), 115295, https://doi.org/10.1016/j.physe.2022.115295G.
[15] A.A. Akinsiku, K.O. Ajanaku, A.A. Adebisi, A. Edobor-Osoh, O. Aladesuyi, T.O. Samson, E.O. Dare, *Momordica charantia* stem extract mediated biogenic synthesis of silver nanoparticles: optical and antimicrobial efficacy, Akinsiku et al 2019 IOP Conf. Ser.: Mater. Sci. Eng. 509 012018. https://doi:10.1088/1757-899X/509/1/012018.
[16] O.P. Bolade, A.A. Akinsiku, S.O., A.B. Williams, N.U. Benson,, Biogenic iron oxide nanoparticles and activated sodium persulphate for hydrocarbon remediation in contaminated soil, Environ. Technol. Innov. 23 (2021), 101719, https://doi.org/10.1016/j.eti.2021.101719.
[17] A.A. Akinsiku, J.A. Adekoya, E.O. Dare, *Nicotiana tabacum* mediated green synthesis of silver nanoparticles and Ag-Ni nanohybrid: optical and antimicrobial efficiency, Indonesia. J. Chem. 21 (1) (2021) 179–199, https://doi.org/10.22146/ijc.56072.
[18] T. Mustapha, N. Misni, N.R. Ithnin, A.M. Daskum, N.Z. Unyah, A review on plants and microorganisms mediated synthesis of silver nanoparticles, the role of plants metabolites and applications. Int J Environ Res Public Health. **19** (2):674 (2022). https://doi: 10.3390/ijerph19020674. PMID: 35055505; PMCID: PMC8775445.
[19] R. Roghini, K. Vijayalakshmi, Phytochemical screening, quantitative analysis of flavonoids and minerals in ethanolic extract of *citrus paradisi*, Int. J. Pharm. Sci. 11 (2018) 4859–4864, https://doi.org/10.4236/oalib.1105439.
[20] T.L. Botha, E.E. Elemike, S. Horn, D.C. Onwudiwe, J.P. Giesy, V. Wepener, Cytotoxicity of Ag, Au and Ag-Au bimetallic nanoparticles prepared using a golden rod (*Solidago canadensis*) plant extract, Sci. Re. 9 (2019) 4169, https://doi.org/10.1038/s41598-019-40816-y.
[21] J.A. Adekoya, M.D. Khan, N. Revaprasadu, Phase transition in $Cu^{2+}xSnS^{3+}y$ ($0 \leq x \leq 2$; $0 \leq y \leq 1$) ternary systems synthesized from complexes of coumarin derived thiocarbamate motifs: optical and morphological properties, RSC Adv. 9 (61) (2019) 35706–35716. ISSN 20462069.
[22] O.C. De Campos, M.P. Layole, F.N. Iheagwam, S.O. Rotimi, S.N. Chinedu, Effect of aqueous extract of M*omordica charantia* on survival, locomotive behaviour and antioxidant status of *Drosophila melanogaster*, Trop. J. Nat. Prod. Res. 5 (1) (2021) 178–181, https://doi.org/10.26538/tjnpr/v5i1.23.
[23] A.O. Abolaji, C.O. Olaiya, O.J. Oluwadahunsi, E.O. Farombi, Dietary consumption of monosodium L-glutamate induces adaptive response and reduction in the life span of *Drosophila melanogaster*, Cell Biochem Funct. 35 (3) (2017) 164–170, https://doi.org/10.1002/cbf.3259.
[24] D.H. Bergey et al., Bergey's Manual of Systematic Bacteriology. Baltimore, MD: Williams & Wilkins, 1984. Print. 1984 edition, 4 volumes. Sci Ref QR81.B46.
[25] J. Ochei, A. Kolhatkar, Medical Laboratory Science, Theory and Practices, Tata McGraw-Hill, New York, 2008, pp. 311–347.
[26] J.A. Kiehlbauch, G.E. Hannett, M. Salfinger, W. Archinal, C. Monserrat, C. Carlyn, Use of the National Committee for Clinical Laboratory Standards guidelines for disk diffusion susceptibility testing in New York state laboratories, J Clin Microbiol. 8 (9) (2000) 3341–3348, https://doi.org/10.1128/JCM.38.9.3341-3348.2000.
[27] Z. Omran, A. Bader, A. Porta, T. Vandamme, N. Anton, Z. Alehaideb, H. El-Said, A. Faidah, A. Essa, M.H. Vassallo, Evaluation of antimicrobial activity of *Triphala* constituents and nanoformulation, Evid.-based Complement. Altern. Med. 6976973 (2000), https://doi.org/10.1155/2020/6976973.
[28] S. Pal, G. De, A new approach for the synthesis of Au−Ag alloy nanoparticle incorporated SiO_2 films, Chem. Mater. 17 (24) (2005) 6161–6166, https://doi.org/10.1021/cm051572r.
[29] Y. Gavamukulya, N. Esther, A.M. Meroka, E.S. Madivoli, H.A. El–Shemy, F. Wamunyokoli, G. Magoma, Green synthesis and characterization of highly stable silver nanoparticles from ethanolic extracts of fruits of Annona muricata, J. Inorg. Organomet. Polym. Mater. 30 (2020) 1231–1242.
[30] Z.U.A. Khan, A. Khan, Y.M. Chen, N.S. Shah, A.U. Khan, N. Muhammad, K. Tahir, H.U. Shah, Z.U. Khan, M. Shakeel, et al., Enhanced antimicrobial, anti-oxidant applications of green synthesized AgNPs- an acute chronic toxicity study of phenolic azo dyes & study of materials surface using x-ray photoelectron spectroscopy, J Photochem. Photobiol. B. 180 (2018) 208–217, https://doi.org/10.1016/j.jphotobiol.2018.02.015.
[31] S. Suresh, Precipitation method and characterization of cobalt oxide nanoparticles, Appl. Phys. A 4 (2017) 123, https://doi.org/10.1007/s00339-017-0786-8).
[32] J.K. Patra, K. Baek, Antibacterial activity and action mechanism of the essential oil from *Enteromorpha linza* L. against foodborne pathogenic bacteria, Molecules 21(3) (2016) 388, https://doi.org/10.3390/molecules21030388.
[33] S. Hull, D.A. Keen, Pressure-induced phase transitions in AgCl, AgBr, and AgILocality: synthetic sample: P = 0.0 GPa, Phase IPhys. Rev. B59 (1999) 750–761.
[34] U.S. Ezealigo, N.B. Ezealigo, S.O. Aisida, F.I. Ezema, Iron oxide nanoparticles in biological systems: Antibacterial and toxicology perspective, JCIS Open. 4, 100027 (2021), ISSN 2666-934X.
[35] K. Sood, J. Kaur, H. Singh, K. Arya, M. Khatri, Comparative toxicity evaluation of graphene oxide (GO) and zinc oxide (ZnO) nanoparticles on *Drosophila melanogaster*, Toxicol. Rep 6 (6) (2019) 768–781, https://doi.org/10.1016/j.toxrep.2019.07.009.
[36] G. Chavez-Esquivel, H. Cervantes-Cuevas, L.F. Ybieta-Olvera, M.T. Castañeda Briones, D. Acosta, J. Cabello, Antimicrobial activity of graphite oxide doped with silver against *Bacillus subtilis, Candida albicans, Escherichia coli*, and *Staphylococcus aureus* by agar well diffusion test: Synthesis and characterization, Mater Sci Eng C Mater Biol Appl. (2021), https://doi.org/10.1016/j.msec.2021.111934.
[37] S. Gurunathan, et al., Enhanced antibacterial and anti-biofilm activities of silver nanoparticles against gram-negative and gram-positive bacteria, Nanoscale Res. Lett. 9 (1) (2014) 373, https://doi.org/10.1186/1556-276X-9-373.
[38] V. Vykoukal, J. Bursik, P. Roupcova, D.A. Cullen, J. Pinkas, Solvothermal hot injection synthesis of core-shell AgNi nanoparticles, J. Alloys Compd. 770 (2019) 377–385, https://doi.org/10.1016/j.jallcom.2018.08.082.
[39] I. Yin, J. Zhang, I. Zhao, M. Mei, Q. Li, C. Chu, The Antibacterial mechanism of silver nanoparticles and its application in dentistry, Int. J. Nanomed. 15 (2020) 2555–2562, http//doi: 10.2147/IJN.S246764. PMID: 32368040; PMCID: PMC7174845.